International Journal of Mass Spectrometry 288 (2009) 36–43

Contents lists available at ScienceDirect

International Journal of Mass Spectrometry

journal homepage: www.elsevier.com/locate/ijms

Resonance ionization mass spectrometry for precise measurements of isotope ratios

Jonathan Levine[a,b,c,*], Michael R. Savina[a,d], Thomas Stephan[a,b], Nicolas Dauphas[a,b,e], Andrew M. Davis[a,b,e], Kim B. Knight[a,b,f], Michael J. Pellin[a,d]

[a] Chicago Center for Cosmochemistry, USA
[b] Department of the Geophysical Sciences, University of Chicago, Chicago, IL 60637, USA
[c] Space Sciences Laboratory, University of California, Berkeley, CA 94720, USA
[d] Materials Science Division, Argonne National Laboratory, Argonne, IL 60439, USA
[e] Enrico Fermi Institute, University of Chicago, Chicago, IL 60637, USA
[f] Lawrence Livermore National Laboratory, Livermore, California 94550, USA

ARTICLE INFO

Article history:
Received 24 April 2009
Accepted 28 July 2009
Available online 18 August 2009

Keywords:
Resonance ionization mass spectrometry
Power broadening
Precision
Chromium isotopes
Presolar grains

ABSTRACT

Resonance ionization mass spectrometry offers extremely high sensitivity and elemental selectivity in microanalysis, but the isotopic precision attainable by this technique has been limited. Measured isotope ratios are sensitive to small fluctuations in the pointing, pulse timing, and wavelength of the resonance lasers. We show that, by minimizing these fluctuations using feedback controls and by power-broadening the optical transitions, we are able to measure chromium isotope ratios with statistics-limited precision better than 1%. Small additional improvements in reproducibility come from careful shaping of the electric field in the region where atoms are photoionized and from minimizing pulse-to-pulse variations in the time-of-flight mass spectrometer through which the photoions travel. The increased reproducibility of isotopic measurements on standard materials has enabled us to detect anomalous chromium isotopic abundances in presolar SiC grains extracted from primitive meteorites.

1. Introduction

Resonance ionization mass spectrometry [1] has long been used for analyses that require high sensitivity and elemental selectivity, and to examine samples that contain very few atoms of an element of interest (e.g., [2]). The technique is especially well suited for applications in cosmochemistry, where sample sizes are small, chemical isolation of an element of interest is either impractical or wasteful, concentrations of many elements are low, and natural isotopic variations can be large. For example, the CHARISMA instrument [3,4] at Argonne National Laboratory is used to identify trace-element isotopic signatures of stellar nucleosynthesis [5–12] in micrometer-sized presolar stardust grains [13–15]. These unique specimens require very small analytical spots and high useful yield, defined as the number of detected atoms of an element of interest normalized by the number of atoms of that element removed from the sample. The useful yield achieved with CHARISMA is ~1%; with the newer SARISA instrument [16,17] the useful yield has exceeded 20%.

In resonance ionization mass spectrometry, atoms are removed from a specimen by ion sputtering or laser desorption, and the ensuing plume of secondary atoms is intercepted by multiple pulsed laser beams tuned to excite successive electronic transitions in a preselected element of interest, promoting the atoms above their ionization thresholds. Atoms of other elements in the cloud of secondary particles, including those that isobarically interfere with the element of interest, are generally transparent to the laser radiation and are therefore hardly ionized. The photoions are extracted and steered through a time-of-flight mass spectrometer and counted. The technique is very sensitive to atoms of the element of interest, for which the ionization efficiency can often approach unity, and is also elementally selective, because the probability of non-resonant ionization of other species can be exceedingly low [18,19].

Efficient ionization of atoms from the cloud of secondary particles requires lasers with high instantaneous spectral power. Some workers (e.g., [20]) achieve this using continuous-wave lasers, with very high spectral purity. Pulsed lasers, despite their inherently wider spectral bandwidth, are more commonly employed in atom-limited applications because of their much higher instantaneous power (for a review, see Wendt and Trautmann [21]). The use of pulsed lasers introduces two important drawbacks, however. First, photoions are created only during the brief laser pulses, and so the duty cycle of pulsed resonance ionization mass spectrometers is necessarily low, compared with continuous-beam instruments.

* Corresponding author. Present address: Department of Physics and Astronomy, Colgate University, Hamilton, New York 13346, USA. Tel.: +1 315 228 6632; fax: +1 315 228 7038.
E-mail address: jlevine@colgate.edu (J. Levine).

1387-3806/$ – see front matter © 2009 Elsevier B.V. All rights reserved.
doi:10.1016/j.ijms.2009.07.013

Second, pulse-to-pulse jitter and long-term drift, especially in laser pointing, pulse timing, and wavelength, limit the attainable reproducibility. Jitter and drift typically limit the isotopic precision of resonance ionization mass spectrometry to a few percent in atom-limited applications (e.g., [22,23]); however, Anderson and Nowicki [24] have recently reported 0.1% precision in an application where extremely high useful yield was not necessary. In this paper we identify the sources of jitter and drift with the largest influences on isotope ratios measured in atom-limited analyses, and we describe the instrumental and procedural improvements we have implemented to obviate them.

Stable and consistent instrumental performance is required, for example, in order to experimentally test models of stellar nucleosynthesis. Presolar grains found in primitive meteorites were formed around late-stage stars that were ancestral to the Sun, and the grains retain isotopic signatures of their stellar sources (for recent reviews see [25,26]). Isotopic analyses of individual presolar grains are diagnostic of the nuclear pathways and reaction conditions that prevail in diverse types of stars, and such measurements impose important constraints on stellar models (e.g., [27]). The most thoroughly studied class of presolar grains are silicon carbide crystals thought to have formed around asymptotic giant branch stars (e.g., [28]). Models of nucleosynthesis in such stars [29,30] predict that these grains should be isotopically anomalous relative to Solar System materials, but the anomalies predicted for isotopes of Fe, Cr, and elements of nearby mass are as small as a few percent. Meaningful experimental tests of these models therefore demand isotopic precision at the level of 1% or better. We shall commonly present isotope ratios in δ units, which are part-per-thousand (‰) deviations from a standard or reference value.

2. Experimental setup

A specimen in the CHARISMA instrument is held under ultra-high vacuum conditions (residual pressure ~1 nTorr), with its surface normal aligned with the axis of the time-of-flight mass spectrometer. Atoms are removed from the specimen surface, photoionized, and steered onto the detector with a 1 kHz repetition rate. This rate affords relatively fast data acquisition while still ensuring that each laser pulse has sufficient energy to saturate its corresponding electronic transition in the cloud of secondary atoms from the specimen. The following paragraphs highlight each of the important components of our apparatus.

The resonance lasers are Nd:YLF-pumped, tunable Ti:sapphire systems that operate over the wavelength range 700–1000 nm, and are tuned by rotating reflection gratings that serve as end-mirrors for each cavity. Depending on the resonance ionization scheme, second-, third-, or fourth-order frequency harmonics of the Ti:sapphire beams may be generated in nonlinear optical crystals, either β-BaB_2O_4 (BBO) or LiB_3O_5 (LBO). A fixed-frequency Nd:YAG laser is often used to ionize the resonantly excited atoms, either in its fundamental mode at 1064 nm, or its second (532 nm) or third (355 nm) frequency harmonics. The Ti:sapphire and Nd:YAG lasers have typical pulse durations of ~15 ns, and are focused into ~1 mm spots above the surface of the specimen.

Immediately before the resonance laser beams reach the analysis point, we remove atoms from the sample surface either by ion sputtering or laser desorption. We use a third-harmonic beam from a Nd:YAG laser for desorption or a liquid-metal ion gun emitting 25 keV Ga^+ ions for sputtering. The atoms removed from the specimen form a small plume whose free expansion rate is determined by the velocities of the desorbed or sputtered atoms.

A small fraction of the atoms leave the sample surface as ions, and because these ions may be of any element, they constitute a source of noise for our measurements. Therefore, as soon as the desorption or the sputtering pulse is finished, the target electrode potential is raised to approximately 4 kV, and positive ions are ejected from the cloud of secondary particles. Neutral atoms in the cloud are unaffected by the high voltage, and the neutral cloud continues to evolve by free expansion. Clouds of secondary neutral particles generated by ion sputtering dissipate relatively rapidly, and only ~300 ns elapses before they become too large to be efficiently intercepted by the resonance and ionization laser beams. With laser desorption, secondary atoms come off the specimen more slowly, and the cloud may expand for ~1000 ns or more before it becomes too rarified for effective resonance ionization. The sample potential is lowered to ground ~100 ns before the resonance lasers encounter the secondary cloud, so that photoionization of secondary neutrals takes place in the absence of strong electric fields.

The resonance laser beams are directed through the secondary cloud, ~100 μm above the specimen surface, where they ionize nearly all of the atoms of the element of interest that they encounter. After ~20 ns the sample potential is pulsed to 2 kV, and the newly generated photoions are accelerated into the time-of-flight mass spectrometer. The photoions are focused in time and space by pulsing a conical extractor electrode to 1.7 kV simultaneously with the sample pulse; a second cone just outside the first is held at ground potential. Effective focusing of the photoions requires that the electric potential vary only slightly over the laser–atom interaction region, with a weak electric field directing positive ions into the time-of-flight mass spectrometer. The shapes and sizes of the sample and extractor electrodes are carefully chosen to shape the electric field for optimal ion transmission and focusing. For additional details of the pulsing sequence, and discussion of isotopic fractionation induced by variations in pulse timings, see Levine et al. [31].

The time-of-flight mass spectrometer contains several pairs of deflection plates, ion lenses, a 2.5 m long flight tube with gridless reflectron (5 m round trip), and a microchannel plate detector. The potential at the back of the reflectron is 2.1 kV, so that the 2 keV photoions are reflected but the direct ions pulsed earlier to 4 kV are not. The data acquisition system for counting individual ions that strike the detector is described by Savina et al. [4].

3. Recent improvements and results

Precise quantification of elemental abundances or isotopic ratios requires that the instrumental fractionation be determined by analyzing standards before and after samples are analyzed. Each measurement may take several hours, and therefore the experimental challenge is to ensure consistent instrumental performance over many hours. Any changes in the intensity, timing, position, or wavelengths of the resonance lasers, in the timing of any of the pulsed elements in the experiment, or in the voltages on any electrode in the time-of-flight mass spectrometer may, in principle, affect the useful yield or fractionate isotopes. Precise measurements therefore require the identification and elimination of the most important sources of variability. In this section, we describe the elements of the experiment to which isotope ratios were most sensitive, and the improvements made to stabilize them.

3.1. Resonance schemes with ultraviolet transitions

As a starting point for this discussion, Fig. 1 shows Fe isotopic ratios measured on a pure Fe foil over the course of a day. Over the 5 h of measurements shown in the figure, the $^{54}Fe/^{56}Fe$ and $^{58}Fe/^{56}Fe$ ratios drifted by >100‰, much more than the statistical uncertainty in any measurement. No comparable drifts in isotope ratios were observed for other elements studied previously, includ-

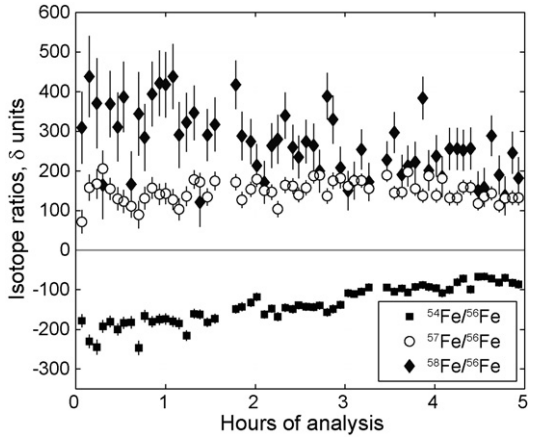

Fig. 1. Drift in measured Fe isotope ratios during analysis of Fe foil. The data were acquired using the two-color resonance ionization scheme for Fe discussed in Section 3.1. Isotope ratios are expressed in δ units, representing part-per-thousand deviations from literature values (i.e., the measurements differ from zero due only to instrumental isotopic fractionation). Error bars represent 1σ statistical errors; the observed drifts are far larger than the statistical uncertainties. During the analyses illustrated here, all the isotope ratios tended toward isotopically lighter values as analyses progressed, but this behavior is not general.

ing Zr, Mo, Ru, and Ba [9–12], but we have subsequently found this behavior among Cr isotopes.

For both Fe and Cr, the changing isotope ratios coincided with small drifts in the wavelengths of the resonance lasers. Our resonance scheme for Fe used 226.021 nm radiation to excite ground-state atoms to the $w^5F_5^o$ state at 44,244 cm^{-1}, followed by 460.702 nm radiation to reach an autoionizing resonance above the ionization threshold of Fe at 63,700 cm^{-1} (laser wavelengths are reported for vacuum propagation). The resonance ionization scheme we used for Cr employed 236.663 nm radiation to excite atoms to the $x^7P_3^o$ level at 42,254 cm^{-1}, followed by 807 nm radiation to ionize the excited atoms. We confirmed, by tuning our first-step lasers back and forth by a few pm in wavelength, that a fractional wavelength change as small as one part in 10^5 was sufficient to change the measured isotope ratios by several tens of percent (Fig. 2). By contrast, Savina et al. [4] showed that wavelength changes at least 10 times larger had an imperceptible effect

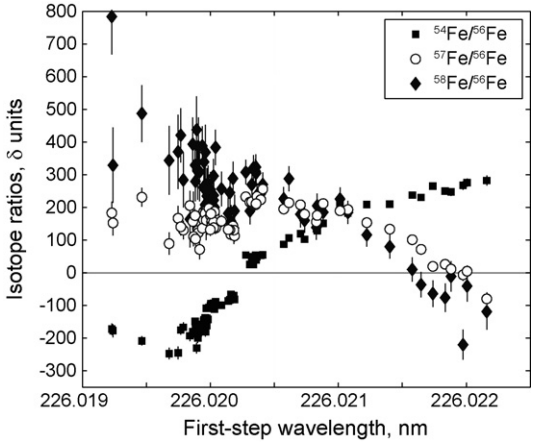

Fig. 2. Dependence of Fe isotope ratios upon the wavelength of the resonance lasers. The abscissa represents the mean wavelength of the first-step resonance laser during each ~2 min analysis. Fluctuations in the mean wavelength of only one part in 10^5 cause factor-of-two changes in the relative isotopic abundances of resonantly ionized Fe atoms from a Fe foil. Small instabilities in the laser wavelength therefore give rise to drifts in isotopic ratios, as seen in Fig. 1. Error bars denote 1σ statistical errors.

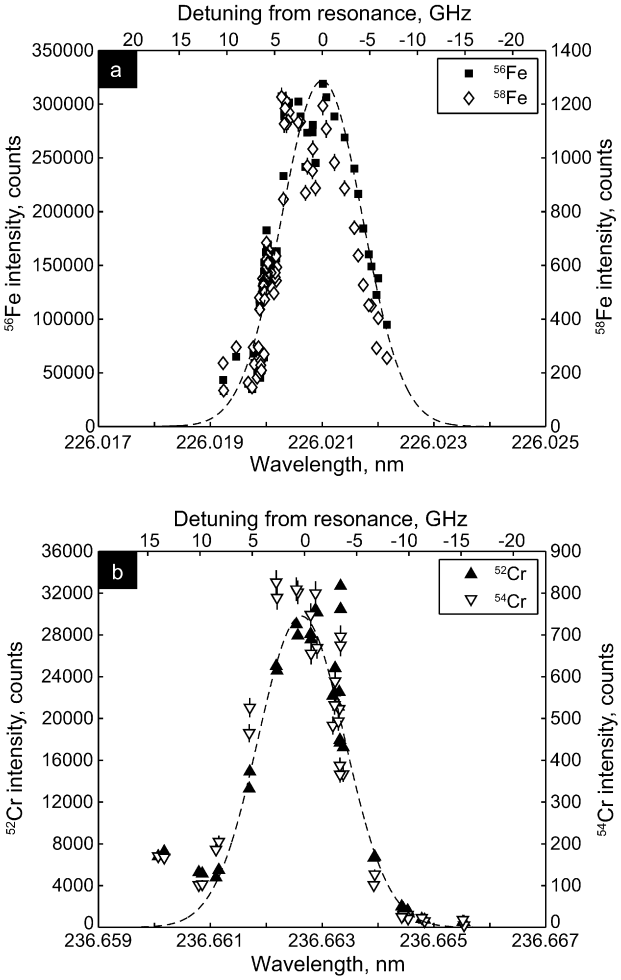

Fig. 3. Wavelength scans across the first-step resonances for Fe (a) and Cr (b). Atoms were efficiently ionized only when the first-step resonance laser was within ±0.001 nm (i.e., ±5 GHz) of the nominal wavelengths of the transitions at 226.021 nm for Fe and 236.663 nm for Cr. Data are approximated by Doppler profiles of full-width 10.0 GHz (Fe) and 9.8 GHz (Cr), shown as dashed curves for the abundant isotopes ^{56}Fe and ^{52}Cr. The resonances for the rare isotopes ^{54}Fe and ^{58}Fe are displaced slightly toward lower wavelength (higher frequencies). Power broadening of these transitions was negligible. Error bars denote 1σ statistical errors; for the abundant isotopes, these are smaller than the symbols in most cases.

on measured ratios of Ba isotopes. Wavelength changes of one part in 10^5 can be caused by thermal expansion of optics induced by ambient temperature fluctuations of only ~1 °C.

We infer the origin of the extreme wavelength sensitivity of Fe and Cr isotopes from observations of the photoion signal as a function of resonance laser wavelength. As seen in Fig. 3, the Fe and Cr resonances were only a few pm wide, corresponding to linewidths of approximately 10 GHz in circular frequency. Linewidths of this magnitude are explained by Doppler broadening of the optical lines: a gas of atoms of mass m at temperature T will have a linewidth (full-width at half-maximum) due to the atoms' line-of-sight velocities with respect to the resonance lasers given approximately by

$$\Delta\nu_{Doppler} = \nu_0\sqrt{8\ln(2)\frac{kT}{mc^2}} \quad (1)$$

where ν_0 is the optical frequency of the transition, kT is the thermal energy, and mc^2 is the atomic rest energy. If we suppose the Fe or Cr atoms in the neutral cloud have velocities characteristic of their boiling temperatures, the Doppler width of the transitions respectively at 226 nm and 236 nm would be 7 GHz (1.3 pm at these

wavelengths). However, because the atoms in the neutral cloud are freely expanding from the sample surface and do not have a Maxwellian distribution of velocities, the analytical expression in Eq. (1) gives only a rough estimate of the Doppler width. Moreover, secondary neutrals created by ion sputtering can have kinetic energies considerably higher than those characteristic of their boiling temperatures. We infer that the observed linewidths of 10 GHz for Fe and Cr are either dominantly or entirely due to Doppler broadening. By contrast, the Ba transition studied by Savina et al. [4] was broadened by additional, non-Doppler mechanisms, such as those we describe below.

Working in a regime in which the Doppler effect is the dominant line-broadening mechanism is disadvantageous for two reasons. First, in an ensemble of atoms subjected to any purely inhomogeneous broadening mechanism, interactions with a weak applied laser field are limited to the subset of atoms whose apparent transition frequency matches that of the laser. In the case of Doppler broadening, only atoms with the appropriate line-of-sight velocity (i.e., 0 if a monochromatic laser is tuned to the nominal transition frequency) will absorb photons from the laser field. Atoms with other line-of-sight velocities are not excited and ionized, and the useful yield is correspondingly low. Second, in the Doppler regime, the velocity segment of the neutral cloud with which the resonance lasers interact is different for each isotope, because of optical isotope shifts. Small fluctuations in the laser frequency can therefore give rise to large variations in the observed abundances of the isotopes. We are unaware of direct measurements of the isotope shifts for the 226.021 nm transition in atomic Fe or the 236.663 nm transition in atomic Cr; however, the isotope shifts for other Cr transitions tabulated by [32] are in the range of 100–3500 MHz (0.06–2 pm for the listed transitions, which are in the blue portion of the spectrum). Even if we conservatively assume that the isotope shift in one of the transitions we excite is only 100 MHz, the measured isotope ratio will be unacceptably sensitive to fluctuations in laser wavelength. This is illustrated in Fig. 4, which shows that, if Doppler broadening is the dominant line-broadening mechanism and plausible optical isotope shifts are assumed, fluctuations of only a few GHz in laser frequency (~1 pm in wavelength) are predicted to cause deviations of tens to hundreds of parts per thousand in measured isotope ratios from an ensemble of atoms.

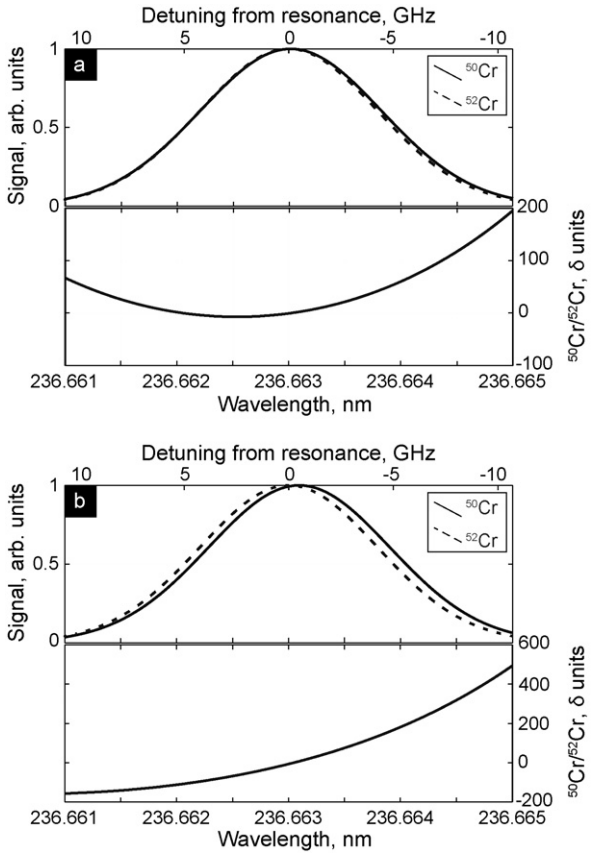

Fig. 4. Idealized dependence of isotope ratios on laser wavelength in the Doppler-broadened regime. We do not know the optical isotope shift for the 236.663 nm resonance of Cr; both 100 MHz (a) and 500 MHz (b) are likely to be underestimates. The Gaussian lineshapes in the upper panels are drawn so that the ^{52}Cr resonance has full-width at half-maximum of 10 GHz. At the same temperature, the ^{50}Cr resonance is broader by the inverse square root of the mass ratio. Lower panels show the isotopic composition of the ensemble of excited atoms, in part-per-thousand deviations from the value obtained with the laser tuned exactly midway between the two resonances. In the Doppler-broadened regime, drifts of only a few parts per million in the laser wavelength give rise to isotopic fractionation of tens to hundreds of parts per thousand, or more if the isotope shifts are larger than illustrated here.

3.2. Power broadening of optical resonances

Useful yield and isotopic reproducibility are greatly improved when we work in a regime in which the spectral linewidth is dominated by (homogeneous) power broadening rather than by (inhomogeneous) Doppler broadening. With sufficient laser power near the resonance frequency, every atom of the element of interest has a reasonable probability of being excited, regardless of its velocity. Moreover, isotopic fractionation is mitigated if the power-broadened linewidth is much greater than the optical isotope shifts for the transition.

We use two strategies for estimating the power-broadened linewidth of our resonances as a function of laser parameters. First, we consider only the two energy levels connected by each transition, and calculate the steady-state excitation by equating the rates of excitation and decay, including both spontaneous and stimulated emission. The steady-state excitation due to monochromatic radiation has Lorentzian shape and full-width at half-maximum given by

$$\Delta\nu_{Power} = \frac{1}{2\pi}\sqrt{A^2 + \frac{2}{\pi c}\left(1+\frac{g_2}{g_1}\right)IB}, \tag{2}$$

where A and B are the Einstein coefficients for spontaneous and stimulated emission; g_2 and g_1 are the multiplicities of the upper and lower states, respectively; I is the instantaneous energy flux of the laser; and c is the speed of light. The B term inside the radical represents the coupling between the atoms and the laser field; for power broadening it is necessary that this term greatly exceed the A^2 term, which represents the natural linewidth. The Einstein A and B coefficients are proportional to one another, and therefore Eq. (2) may be restated as

$$\Delta\nu_{Power} = \frac{1}{2\pi}\sqrt{A^2 + \frac{c^2}{2\pi h\nu_0^3}\left(1+\frac{g_2}{g_1}\right)IA}, \tag{3}$$

where h is Planck's constant. The approximation of an isolated pair of coupled states is nearly valid in some fluorescence experiments; however, the physics of resonance ionization is more complicated because each pair of energy levels is coupled to additional discrete states and/or the ionization continuum, and thus no steady state is reached. For this reason, Eq. (3) gives only an order-of-magnitude estimate of the power-broadened linewidths observed in a resonance ionization experiment. Nevertheless, Eq. (3) shows that power broadening is favored by strong transitions, high laser power, high transition frequency (i.e., low wavelength), and high multiplicity of the excited state.

We make more realistic linewidth estimates by numerical integration of the equation of motion for the density matrix rep-

resenting an ensemble of atoms subjected to multiple laser fields. We simplify the calculation by (1) assuming that each laser consists of a monochromatic carrier signal whose envelope may be slowly modulated, (2) making the rotating wave approximation for each resonant interaction (including the coherences between non-consecutive states), (3) requiring that each laser interact only with atoms in a single pair of states, and (4) representing the ionization process by a simple rate equation. We further assume that collisions among the atoms in the freely expanding secondary cloud are infrequent enough to be negligible, and we adopt the values of Einstein *A* coefficients tabulated by Ralchenko et al. [33]. The results of these calculations depend on the cross-section for photoionization from the excited state, which we estimate to be tens of Mbarn (by contrast, strong resonant transitions have cross-sections for absorption and stimulated emission of tens to hundreds of Gbarn). Notwithstanding this important uncertainty, the numerical integrations give linewidth estimates that are broadly consistent with the steady-state solution for each two-level subsystem. The near agreement is partly due to rapid decay of the quantum coherences if the laser frequencies are on the wings of the resonance, where the generalized Rabi flopping period is long compared with the rise time of a laser pulse. Once the coherences have decayed, the dynamical evolution can be approximated by rate equations, like those giving rise to Eq. (3).

The 226.021 nm transition in Fe and the 236.663 nm transition in Cr had been excited by frequency-quadrupled Ti:sapphire lasers at 904.084 nm and 946.650 nm, respectively. The fundamental Ti:sapphire energy was approximately 1000 μJ per pulse, but frequency-quadrupling is an inherently inefficient process, and we obtained only 15–45 μJ per pulse in the frequency-quadrupled beams. If a laser is in perfect tune with an atomic resonance, even this low intensity is sufficient to saturate a transition. Nevertheless, the saturation is not robust to jitter and drift in the laser wavelengths. The power-broadened linewidths we estimate from Eq. (3) for these resonances in Fe and Cr (assuming instantaneous energy flux $I = 4\ \mathrm{kW\,mm^{-2}}$, for 15 ns pulses delivering 45 μJ through a spot with 1 mm diameter) are only 3.5 GHz, or less than 1 pm in wavelength. Typical pulse-to-pulse frequency jitter in our laboratory was approximately 8 GHz (1.5 pm in wavelength), and frequency drifts were commonly 10–20 GHz per hour (~2–4 pm per hour in wavelength). Most laser pulses, therefore, excited their transitions only weakly, giving rise to low useful yields and, in conjunction with the optical isotope shifts, to large isotopic fractionations.

As noted above (Section 3.1), Savina et al. [4] showed that measured Ba isotope ratios were robust to small changes in laser wavelengths. The resonance ionization of Ba, and of other elements we have examined (Zr, Mo, and Ru; e.g., [9–12]), did not require frequency-quadrupled lasers, but rather used Ti:sapphire fundamental beams or their second or third harmonics. Eq. (3) shows two reasons why linewidths of these transitions are more easily power broadened. First, the power-broadened linewidth increases with increasing energy flux in the laser beam, which is larger for lower order harmonics than for frequency-quadrupled beams. Second, the power-broadened linewidth depends on $\nu_0^{-3/2}$, and again favoring lower-order frequency harmonics (i.e., higher wavelengths).

To maximize useful yields and to minimize the variations in measured isotope ratios due to laser wavelength instability, we adopted a resonance ionization scheme for Cr in which the resonance widths are indeed dominated by power broadening. The new resonance scheme uses three photons, each with modest energy, to impart the 6.77 eV ionization energy to neutral Cr atoms, instead of relying on ultraviolet photons to populate high-lying excited states. This has the added advantage of reducing non-resonant photoionization of interfering species such as SiC_2, which had been the largest source of isobaric interference for ^{52}Cr, ^{53}Cr, and ^{54}Cr. The three-photon scheme uses 427.600 nm radiation to excite Cr atoms from their ground state to the $z^7P_3^o$ level at 23386 $\mathrm{cm^{-1}}$, followed by 449.296 nm radiation to promote the excited atoms to the f^7S_3 level at 45643 $\mathrm{cm^{-1}}$, from which they are ionized by an intense 1064 nm beam from a Nd:YAG laser. The 427 nm and 449 nm beams are generated by frequency-doubling Ti:sapphire lasers at 855 nm and 898 nm, with >100 μJ per pulse in the frequency-doubled beams. The power broadening of the transitions is improved both because we avoid the power losses in frequency-quadrupling, and also because of the $\nu_0^{-3/2}$ dependence of the linewidth in the dominant term in Eq. (3). From Eq. (3), we estimate linewidths of 28 GHz (17 pm) and 12 GHz (8 pm) for the respective transitions. For comparison, the Doppler widths of these transitions (at 3000 K) are approximately 3.8 GHz (2.5 pm). In this scheme, therefore, the available laser power is sufficient to power broaden the two resonances. Fig. 5 shows that the linewidth estimate from Eq. (3) agrees with our observations of the 427.600 nm resonance.

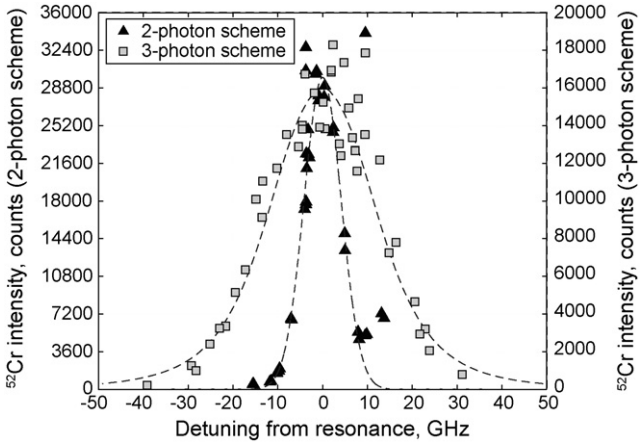

Fig. 5. Wavelength scans across the first-step resonances for Cr using two- and three-photon resonance ionization schemes. Whereas the 236.663 nm resonance in the two-photon case (triangular symbols) is dominated by Doppler broadening (full-width at half-maximum 10 GHz or 0.002 nm), the 427.600 nm resonance in the three-photon case (square symbols) is power broadened to 28 GHz (0.017 nm). We simulated the latter data by numerically integrating the interactions between the Cr atoms and all three laser beams, with the following parameters: beam diameters 1 mm, pulse duration 15 ns, pulse energies 100 μJ for the first two resonance lasers and 4000 μJ for the ionization laser, and ionization cross-section from the second excited state 20 Mbarn. Doppler broadening of the 427.600 nm transition, expected to be 3.8 GHz or 0.002 nm, was neglected. 1σ error bars are in most cases smaller than the symbols.

3.3. Feedback stabilization of resonance lasers

In addition to choosing resonance schemes that, because of power broadening, are relatively insensitive to fluctuations in the wavelengths of the resonance lasers, we have also implemented a feedback control system to minimize wavelength fluctuations. Our system monitors the wavelengths of our tunable lasers using a multichannel wavelength meter (HighFinesse-Ångstrom model WS7). The wavelength of each tunable laser is measured every ~1 s, and any drift is compensated for by rotating the reflection gratings in the corresponding laser cavity using a piezoelectric actuator. The actuators (New Focus model 8310 closed loop "Picomotors") have 63 nm linear resolution, enabling us to rotate the gratings in steps of ~1 μrad, and thus to change the wavelengths of the Ti:sapphire lasers by ~1 pm. Second- and third-harmonic beams are tunable, therefore, in steps of 0.5 pm and 0.3 pm, respectively. Moreover, we have eliminated the wavelength drifts our lasers had suffered; the feedback control system now maintains the laser frequency to within ~0.8 GHz (i.e., 0.5 pm for a second-harmonic beam) indefinitely.

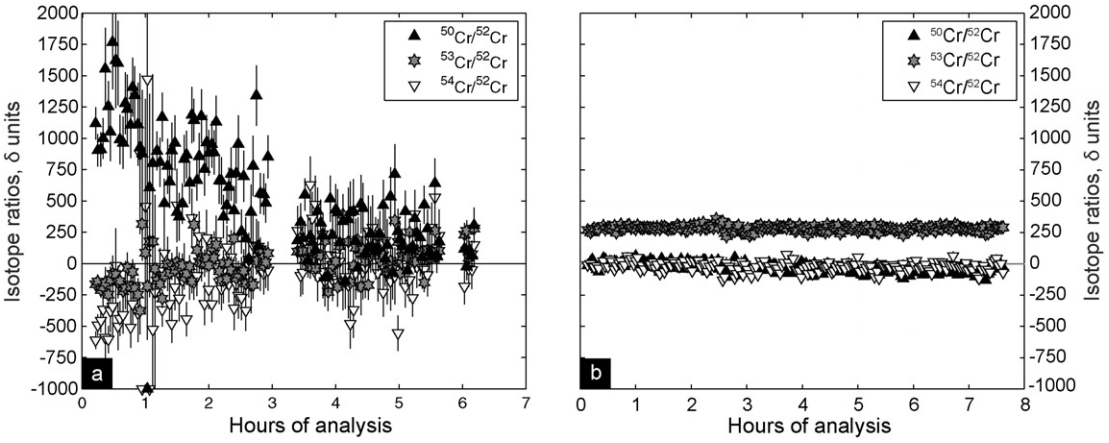

Fig. 6. Drift in measured Cr isotope ratios during analysis of Cr metal. (a) Data acquired using the two-photon resonance ionization scheme for Cr and without feedback control of laser wavelength. All measured isotope ratios drifted by factors of ~2 over the day. (b) Data obtained using the three-color resonance ionization scheme for Cr and with stabilized laser wavelength, timing, and pointing. More efficient ionization using the three-color resonance scheme also led to higher count rates, and therefore smaller statistical uncertainties. Drift in the isotope ratios is reduced to ~10‰ per hour. Error bars denote 1σ statistical errors.

Frequency stabilization at the <1 GHz level and power broadening of all laser transitions eliminated what were by far the largest sources of drift in our measurements of Cr isotope ratios. Doing so revealed the next largest sources of error, which were drifts in the timing of the laser pulses and in the position where the laser beams intercept the cloud of secondary particles. Timing and pointing instabilities can affect isotope ratios of the atoms intercepted by the lasers, because free expansion of the cloud is generally faster for light isotopes than for heavy ones, and thus at any time the front of the expanding cloud is isotopically lighter than the center or rear. To avoid drifts in laser pulse timing, we have implemented a feedback loop including a programmable logic controller (LabSmith model LC880) whose inputs include photodiode signals from the lasers and whose outputs are used to trigger successive laser pulses. We also stabilized the laser pointing by controlling the temperature of the laser table and optics with regulated infrared heaters (Kalglo model MR-1215) that maintain a constant temperature (0.3 °C tolerance) throughout our Ti:sapphire cavities. To ensure that the position of the laser beams where they intercept the secondary cloud is stable at the 100 μm level, the drift in beam pointing in the Ti:sapphire cavities must be smaller than ~30 μrad. We now achieve this level of pointing stability.

These improvements in laser power and stability have dramatically improved the precision and reproducibility in our measurements of isotope ratios. Fig. 6 contrasts sets of repeated analyses of Cr isotopes from a Cr metal target, measured before and after these improvements. Higher photoionization efficiency has led to higher count rates and smaller statistical uncertainties. In place of factor-of-two drifts over a day of measurements, we now find drifts that are smaller than 10‰ per hour. Given the count rates we can tolerate in our experiments, such small drifts allow us to make isotopic measurements with <10‰ precision and with repeated analyses in statistical agreement ($\chi^2 \approx 1$ per degree of freedom).

4. Application to presolar grains

With the increased isotopic precision, we have made the first measurements of Cr isotopes in presolar SiC grains [34]. The grains we analyzed were extracted from the Murchison meteorite using chemical procedures designed to keep them free of potential Cr contamination. The standard procedure for isolating presolar SiC grains involves kerogen oxidation with chromic acid and density separation with sodium ploytungstate [35], which can contaminate the grains with terrestrial Cr and W [36]. For the purpose of measuring the isotopic composition of Cr and W native to the grains, a new batch of SiC grains (RWB) was therefore prepared avoiding these reagents. The starting material was a residue extracted from the Murchison meteorite (A14.3; 8.60 mg representing 3.3 g of bulk meteorite) following the treatment described by Lewis et al. [37] (A14.3 corresponds to the bulk of 2C10c, 2C10m, and 2C10f before size separation). The residue was separated by sedimentation into four fractions differing in grain size (nominally <1.5 μm, 1.5–3 μm, 3–6 μm, and >6 μm). Each size fraction was treated with concentrated H_2SO_4 at 200 °C for 12 h, $HClO_4$ at 195 °C for 4 h, a solution of 10 M HF and 1.2 M HCl at 20 °C for 12 h, and $HClO_4$ at 180 °C for 3 h. The SiC grains used in this study are from the RWB6- series, which contains grains that are, for the most part, 2–4 μm in size. A fraction of the RWB6- grains (RWB6-1) were mounted on a high purity gold foil by depositing them from a suspension. For standardization purposes, synthetic Cr_3C_2 grains, whose isotopic composition we take to be that of Solar System materials, were deposited on the same mount with the assistance of R.S. Lewis.

Cr isotopes are difficult to measure in presolar SiC grains for at least two reasons. First, the small size of the grains and the low concentration of Cr within them (~1 part per million [36]) imply that each grain may contain only a few million Cr atoms. Second, the isotopes ^{50}Cr and ^{54}Cr are isobaric with atomic species such as ^{50}Ti, ^{50}V, and ^{54}Fe, whose abundances can be comparable or greater. Molecular species such as SiC_2 can also isobarically interfere with Cr isotopes. Four-isotope measurements of Cr therefore require the high sensitivity and elemental selectivity of resonance ionization mass spectrometry. Moreover, models of nucleosynthesis in asymptotic giant branch stars [29,30] predict only modest anomalies in the abundances of Cr isotopes relative to Solar System materials (depletions of 20–40‰ in $^{50}Cr/^{52}Cr$, enrichments of 1–3‰ in $^{53}Cr/^{52}Cr$, and enrichments of 80–200‰ in $^{54}Cr/^{50}Cr$), so meaningful experimental tests of these models must have high isotopic accuracy and precision.

Fig. 7 shows our first measurements of Cr isotopes in presolar SiC grains. We are continuing to analyze more grains, and we will describe the astrophysical significance of our observations elsewhere. For our present purposes, we simply state that the ensemble of presolar SiC grains is isotopically distinct from Solar System materials, represented here by the synthetic Cr_3C_2 grains that were deposited alongside the presolar SiC grains. The $^{50}Cr/^{52}Cr$ and $^{53}Cr/^{52}Cr$ ratios of nearly all the SiC grains are low relative to the same ratios in the Cr_3C_2 standards, with a mean depletion of

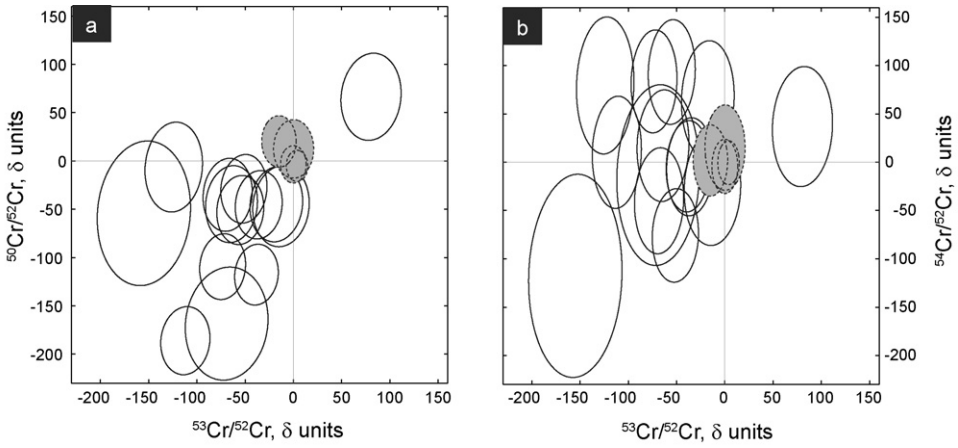

Fig. 7. Abundances of Cr isotopes in 14 presolar SiC grains. Isotope ratios are expressed in part-per-thousand deviations from the mean of analyses on synthetic Cr_3C_2 standards (shaded ellipses). (a) $^{50}Cr/^{52}Cr$ and $^{53}Cr/^{52}Cr$ ratios of nearly all the presolar SiC grains (open ellipses) are lower than those of Solar System materials, with a mean depletion (or, a mean enrichment of ^{52}Cr) of ~60‰. (b) $^{54}Cr/^{52}Cr$ vs. $^{53}Cr/^{52}Cr$ ratios of the presolar SiC grains (open ellipses). The $^{54}Cr/^{52}Cr$ ratios of the presolar grains are indistinguishable from those of the synthetic Cr_3C_2 standards. Ellipses contour 1σ confidence levels. The precision of the presolar grain measurements is limited by counting statistics rather than by the reproducibility of the standard measurements.

~60‰. The $^{54}Cr/^{50}Cr$ ratio of most SiC grains is consistent with the Solar System value, but anomalies of ±50‰ cannot be ruled out. The uncertainties in our measurements, though still somewhat large, are dominated by the counting statistics of the Cr atoms in the SiC grains, and not by instrumental effects.

5. Conclusions

Reproducible measurements of isotope ratios by resonance ionization mass spectrometry require that the laser interactions with the desorbed atoms be robust to variations in laser pointing, pulse time, and especially wavelength. It is advantageous to excite transitions that can be substantially power broadened by the resonance lasers, both for maximizing useful yields and for minimizing isotopic fractionations caused by optical isotope shifts. Resonance ionization schemes that employ high-order frequency-harmonic laser beams are unfavorable for power broadening because of the low powers available and because of the strong inverse dependence of the power-broadened linewidth on the transition frequency. We obtain statistically limited measurements of isotope ratios with <10‰ precision by (1) choosing a resonance ionization scheme for which the resonances can be substantially power broadened, (2) stabilizing the wavelength and pulse timing of the resonance lasers with feedback controls, and (3) stabilizing the position of the laser beams where they intercept the secondary cloud.

There are several resonance ionization mass spectrometry experiments in cosmochemistry that are enabled by the high precision and reproducibility demonstrated here. We have used Cr isotopes to illustrate the improved performance of our apparatus and have made the first experimental tests of stellar nucleosynthesis models of this element, analyzing presolar SiC grains extracted from meteorites and finding anomalous isotope abundances. We also plan to measure the Fe isotopic composition of presolar SiC grains: as for Cr isotopes, the predictions of nucleosynthesis models [29,30] for Fe isotopes are modest depletions of the light isotope ^{54}Fe relative to the intermediate-mass isotopes ^{56}Fe and ^{57}Fe, and for a more marked enrichment of the neutron-rich ^{58}Fe. Our measurement of Fe isotopes will enable a comparison with the recent measurements by Marhas et al. [38] by secondary ion mass spectrometry; however, resonance ionization measurements will allow measurement of the astrophysically interesting isotope ^{58}Fe in addition to the other isotopes. In the future, we intend to search for the as-yet-unidentified carrier phase of anomalous ^{54}Cr in carbonaceous chondrites and other meteorites (e.g., [39]), and to use ^{58}Fe abundances to probe the origin of amorphous silicates in interplanetary dust particles [40,41].

With the uncertainties of our trace-element measurements in presolar grains now limited by counting statistics at the level of a few percent, further improvements will need to come from improved sensitivity. Though we have not precisely measured the useful yield of Cr directly in this experiment, it is broadly consistent with the value of ~1% obtained with CHARISMA in other work. Analysis with SARISA, or with the ion nanoprobe under construction at the University of Chicago [42], should improve the useful yields by a factor of 20 or more, and thereby reduce statistical uncertainty by at least a factor of four. The increased isotopic precision of resonance ionization mass spectrometry will also be useful in measurements that are not limited by the number of available atoms, such as nuclear forensics experiments.

Acknowledgements

We are grateful for the assistance of R.S. Lewis in preparing the sample mount, and also to C.E. Tripa, I.V. Veryovkin, and A. Zinovev. We wish to thank R. Santra, W. Happer, and D. Budker for useful discussions. Our work is supported by NASA through grants NNG06-GF19G, NNG09-AG39G, and NNX07-AL94G and work orders W-19895 and W-10091, and by the US Department of Energy, Office of Basic Energy Sciences under contract DEAC02-06CH11357.

References

[1] J.D. Fassett, L.J. Moore, J.C. Travis, J.R. DeVoe, Laser resonance ionization mass spectrometry, Science 230 (1985) 262–267.
[2] M.J. Pellin, C.E. Young, W.F. Calaway, J.W. Burnett, B. Jørgensen, E.L. Schweitzer, D.M. Gruen, Sensitive, low damage surface analysis using resonance ionization of sputtered atoms, Nuclear Instruments and Methods in Physics Research B18 (1987) 446–451.
[3] Z. Ma, R.N. Thompson, K.R. Lykke, M.J. Pellin, A.M. Davis, New instrument for microbeam analysis incorporating submicron imaging and resonance ionization mass spectrometry, Reviews of Scientific Instruments 66 (1995) 3168–3176.
[4] M.R. Savina, M.J. Pellin, C.E. Tripa, I.V. Veryovkin, W.F. Calaway, A.M. Davis, Analyzing individual presolar grains with CHARISMA, Geochimica et Cosmochimica Acta 67 (2003) 3215–3225.
[5] G.K. Nicolussi, A.M. Davis, M.J. Pellin, R.S. Lewis, R.N. Clayton, S. Amari, *s*-Process zirconium in presolar silicon carbide grains, Science 277 (1997) 1281–1283.
[6] G.K. Nicolussi, M.J. Pellin, R.S. Lewis, A.M. Davis, S. Amari, R.N. Clayton, Molybdenum isotopic composition of individual presolar silicon carbide grains from the Murchison meteorite, Geochimica et Cosmochimica Acta 62 (1998) 1093–1104.

[7] G.K. Nicolussi, M.J. Pellin, R.S. Lewis, A.M. Davis, R.N. Clayton, S. Amari, Strontium isotopic composition in individual circumstellar silicon carbide grains: a record of *s*-process nucleosynthesis, Physical Review Letters 81 (1998) 3583–3586.
[8] G.K. Nicolussi, M.J. Pellin, R.S. Lewis, A.M. Davis, R.N. Clayton, S. Amari, Zirconium and molybdenum in individual circumstellar graphite grains: new isotopic data on the nucleosynthesis of heavy elements, Astrophysical Journal 504 (1998) 492–499.
[9] M.R. Savina, A.M. Davis, C.E. Tripa, M.J. Pellin, R.N. Clayton, R.S. Lewis, S. Amari, R. Gallino, M. Lugaro, Barium isotopes in individual presolar silicon carbide grains from the Murchison meteorite, Geochimica et Cosmochimica Acta 67 (2003) 3201–3214.
[10] M.R. Savina, A.M. Davis, C.E. Tripa, M.J. Pellin, R. Gallino, R.S. Lewis, S. Amari, Extinct technetium in silicon carbide stardust grains: implications for stellar nucleosynthesis, Science 303 (2004) 649–652.
[11] J.G. Barzyk, M.R. Savina, A.M. Davis, R. Gallino, M.J. Pellin, R.S. Lewis, S. Amari, R.N. Clayton, Multi-element isotopic analysis of single presolar SiC grains, New Astronomy Reviews 50 (2006) 587–590.
[12] J.G. Barzyk, M.R. Savina, A.M. Davis, R. Gallino, F. Gyngard, S. Amari, M.J. Pellin, R.S. Lewis, R.N. Clayton, Constraining the ^{13}C neutron source in AGB stars through isotopic analysis of trace elements in presolar SiC, Meteoritics and Planetary Science 42 (2007) 1103–1119.
[13] R.S. Lewis, T. Ming, J.F. Wacker, E. Anders, E. Steel, Interstellar diamonds in meteorites, Nature 326 (1987) 160–162.
[14] T. Bernatowicz, G. Fraundorf, T. Ming, E. Anders, B. Wopenka, E. Zinner, P. Fraundorf, Evidence for interstellar SiC in the Murray carbonaceous meteorite, Nature 330 (1987) 728–730.
[15] E. Zinner, T. Ming, E. Anders, Isotopic anomalies of Si, C, N, and noble gases in interstellar silicon carbide from the Murray meteorite, Nature 330 (1987) 730–732.
[16] I.V. Veryovkin, W.F. Calaway, J.F. Moore, M.J. Pellin, D.S. Burnett, A new time-of-flight instrument for quantitative surface analysis, Nuclear Instruments and Methods in Physics Research B219–B220 (2004) 473–479.
[17] I.V. Veryovkin, W.F. Calaway, C.E. Tripa, J.F. Moore, A. Wucher, M.J. Pellin, Laser post-ionization secondary neutral mass spectrometry for ultra-trace analysis of samples from space return missions, Nuclear Instruments and Methods in Physics Research B241 (2005) 356–360.
[18] G.S. Hurst, M.H. Nayfeh, J.P. Young, One-atom detection using resonance ionization spectroscopy, Physical Review A15 (1977) 2283–2292.
[19] G.S. Hurst, M.G. Payne, S.D. Kramer, J.P. Young, Resonance ionization spectroscopy and one-atom detection, Reviews of Modern Physics 51 (1979) 767–819.
[20] I.K. Perera, I.C. Lyon, G. Turner, Isotope ratio measurements in strontium using two-photon two-colour resonance ionization mass spectrometry, Journal of Analytical Atomic Spectrometry 10 (1995) 273–280.
[21] K. Wendt, N. Trautmann, Recent developments in isotope ratio measurements by resonance ionization mass spectrometry, International Journal of Mass Spectrometry 242 (2000) 161–168.
[22] J. Maul, K. Eberhardt, G. Huber, S. Karpuk, G. Passler, M.C. Roca-Saiz, I. Strachnov, N. Trautmann, K. Wendt, Multi-color resonance ionization of laser ablated gadolinium at high laser power, Optics Communications 256 (2005) 364–372.
[23] S.L. Ziegler, B.A. Bushaw, Ultratrace uranium fingerprinting with isotope selective laser ionization spectrometry, Analytical Chemistry 80 (2008) 6029–6033.
[24] F.S. Anderson, K. Nowicki, In-situ LDRIMS geochronometry for the Moon and Mars, Lunar and Planetary Science Conference 40 (2009) (abstract) 2290.
[25] D.D. Clayton, L.R. Nittler, Astrophysics with presolar stardust, Annual Reviews of Astronomy and Astrophysics 42 (2004) 39–78.
[26] E. Zinner, Presolar grains, in A.M. Davis (Ed.) Meteorites, Planets, and Comets, vol. 1 of H.D. Holland and K.K. Turekian (Eds.) Treatise on Geochemistry, 2nd Ed. Elsevier, Oxford, 2007. Published electronically at http://www.sciencedirect.com/science/referenceworks/9780080437514, doi:10.1016/B0-08-043751-6/01144-0.
[27] M. Lugaro, A.M. Davis, R. Gallino, M.J. Pellin, O. Straniero, F. Käppeler, Isotopic compositions of strontium, zirconium, molybdenum, and barium in single presolar SiC grains and asymptotic giant branch stars, Astrophysical Journal 593 (2003) 486–508.
[28] E. Zinner, Stellar nucleosynthesis and the isotopic composition of presolar grains from primitive meteorites, Annual Reviews of Earth and Planetary Science 26 (1998) 147–188.
[29] R. Gallino, C. Arlandini, M. Busso, M. Lugaro, C. Travaglio, O. Straniero, A. Chieffi, M. Limongi, Evolution and nucleosynthesis in low-mass asymptotic giant branch stars. II. Neutron capture and the *s*-process, Astrophysical Journal 497 (1998) 388–403.
[30] M. Busso, R. Gallino, D.L. Lambert, C. Travaglio, V.V. Smith, Nucleosynthesis and mixing on the asymptotic giant branch. III. Predicted and observed *s*-process abundances, Astrophysical Journal 557 (2001) 802–821.
[31] J. Levine, M. Savina, T. Stephan, M. Pellin, Improvements in RIMS isotopic precision: application to in situ atom-limited analyses, in: T. Iguchi, K. Watanabe (Eds.), 4th International Conference on Laser Probing—LAP 2008, American Institute of Physics Conference Proceedings 1104, 2009, pp. 90–95.
[32] B. Furmann, A. Jarosz, D. Stefańska, J. Dembczyński, E. Stachowska, Isotope shift in chromium, Spectrochimica Acta B60 (2005) 33–40.
[33] Y. Ralchenko, A.E. Kramida, J. Reader, NIST ASD Team, NIST Atomic Spectra Database (version 3.1.5), National Institute of Standards and Technology, Gaithersburg, Maryland, 2008, Published electronically at http://physics.nist.gov/asd3.
[34] J. Levine, M.R. Savina, N. Dauphas, A.M. Davis, B.H. Isselhardt, K.B. Knight, R.S. Lewis, M.J. Pellin, T. Stephan, First four-isotope measurements of chromium in presolar SiC grains, Lunar and Planetary Science Conference 40 (2009) 1982, abstract.
[35] S. Amari, R.S. Lewis, E. Anders, Interstellar grains in meteorites. I. Isolation of SiC, graphite, and diamond; size distribution of SiC and graphite, Geochimica et Cosmochimica Acta 58 (1994) 459–470.
[36] K.B. Knight, S.R. Sutton, M. Newville, A.M. Davis, N. Dauphas, R.S. Lewis, S. Amari, I.M. Steele, M.R. Savina, M.J. Pellin, Trace element determinations in presolar SiC grains by synchrotron X-ray fluorescence: commencement of a coordinated multimethod study, Lunar and Planetary Science Conference 39 (2008) 2135, abstract.
[37] R.S. Lewis, L. Alaerts, J.-I. Matsuda, E. Anders, Stellar condensates in meteorites: isotopic evidence from noble gases, Astrophysical Journal Letters 234 (1979) L165–L168.
[38] K.K. Marhas, S. Amari, F. Gyngard, E. Zinner, R. Gallino, Iron and nickel isotopic ratios in presolar SiC grains, Astrophysical Journal 689 (2008) 622–645.
[39] A. Trinquier, J.-L. Birck, C.J. Allègre, Widespread ^{54}Cr heterogeneity in the inner Solar System, Astrophysical Journal 655 (2007) 1179–1185.
[40] A.J. Westphal, J.P. Bradley, Formation of glass with embedded metal and sulfides from shock-accelerated crystalline dust in superbubbles, Astrophysical Journal 617 (2004) 1131–1141.
[41] A.J. Westphal, A.M. Davis, J. Levine, M.J. Pellin, M.R. Savina, GEMS at the galactic cosmic ray source, Space Science Reviews 130 (2007) 451–456.
[42] A.M. Davis, T. Stephan, I.V. Veryovkin, M.J. Pellin, M.R. Savina, The ion nanoprobe: a new instrument for studying the isotopic and elemental composition of the solar system and beyond at the few-nanometer scale, Lunar and Planetary Science Conference 40 (2009) 2472, abstract.